Field-induced single ion magnet behaviour of discrete and one-dimensional complexes containing [bis(1-methylimidazol-2-yl)ketone]-cobalt(ii) building units

Juan-Ramón Jiménez, Buqing Xu, Hasnaa El Said, Yanling Li, Jurgen von Bardeleben, Lise-Marie Chamoreau, Rodrigue Lescouëzec, Sergiu Shova, Diana Visinescu, Maria-Gabriela Alexandru, et al.

ARTICLE

Field-induced Single Ion Magnet behaviour in discrete and one-dimensional complexes containing the bis(1-methylimidazol-2-yl)ketone]-cobalt(II) building units

Received 00th January 20xx.
Accepted 00th January 20xx

DOI: 10.1039/x0xx00000x

Juan-Ramón Jiménez,[a] Buqing Xu [a], Hasnaa El Said,[a] Yanling Li,*[a] Jurgen von Bardeleben,[b] Lise-Marie-Chamoreau,[a] Rodrigue Lescouëzec,[a] Sergiu Shova,[c] Diana Visinescu,[d] Maria-Gabriela Alexandru,*[e] Joan Cano[f] and Miguel Julve*[f]

We describe herein the first examples of six-coordinate Co^{II} Single-Ion Magnets (SIMs) based on the β-diimine ^{Me}bik ligand [^{Me}bik = bis(1-methylimidazol-2-yl)ketone]: two mononuclear $[Co^{II}(^{R}bik)_2L_2]$ complexes and one mixed-valence $\{Co^{III}_2Co^{II}\}_n$ chain of formula $[Co^{II}(^{Me}bik)(H_2O)(dmso)(\mu\text{-}NC)_2Co^{III}_2(\mu\text{-}2,5\text{-}dpp)(CN)_6]_n \cdot 1.4nH_2O$ (**3**) [L = NCS (**1**), NCSe (**2**) and 2,5-dpp = 2,5-bis(2-pyridyl)pyrazine (**3**)]. Two bidentate ^{Me}bik molecules plus two monodentate *N*-coordinate pseudohalide groups in *cis* positions build somewhat distorted octahedral surroundings around the high-spin cobalt(II) ions in **1**-**2**. The diamagnetic $[Co^{III}_2(\mu\text{-}2,5\text{-}dpp)(CN)_8]^{2-}$ metalloligand coordinates the paramagnetic $[Co^{II}(^{Me}bik)(H_2O)(dmso)]^{2+}$ complex cations in a bis-monodentate fashion to afford neutral zigzag heterobimetallic chains in **3**. *Ab-initio* calculations, cryomagnetic dc (2.0-300 K) and ac (2.0-12 K) measurements as well as EPR spectroscopy for **1**-**3** show the occurrence of magnetically isolated high-spin cobalt(II) ions with *D* values of 59.84 – 89.90 (**1**), 66.32 – 93.90 (**2**) and 70.49 – 127.20 cm^{-1} (**3**) and field-induced slow relaxation of the magnetization, being thus new examples of SIMs with transversal magnetic anisotropy. The analysis of their relaxation dynamics reveals that the relaxation of the magnetization occurs by Raman (with values of the *n* parameter covering the range 6.0-6.8) and direct spin-phonon processes.

Introduction

In the last decades, molecular chemistry turned out to be an efficient approach to design materials showing original magnetic properties that are not encountered otherwise in alloys or oxide-based magnetic materials.[1–3] In particular, the molecular chemistry approach has proved to be successful for the design of new bistable magnetic systems. For example, strong research efforts have been devoted in the last years to the study of the so-called single-molecule magnets (SMMs),[4] single-chain magnets (SCMs),[5,6] or single-ion magnets (SIMs).[7,8] In these low-dimensional mono- (SIM) or poly-metallic (SMMs or SCMs) complexes, the existence of a large axial anisotropy (*D*) in the spin ground state allows stabilizing the magnetic moment in one preferred direction. Once oriented with a strong magnetic field, the magnetic moments can be trapped in that direction at low temperature. The application of intense magnetic fields in opposite direction are necessary to reverse the magnetization leading to magnetic hysteresis and bistability.[9] Spin-crossover complexes[3] or complexes showing valence tautomerism[10] represent another important class of bistable molecular materials. Typically, in these systems, external stimuli (such as temperature, pressure, light irradiation, electric and magnetic fields) allow switching between two electronic configurations that are close in energy. The change of electronic state does not

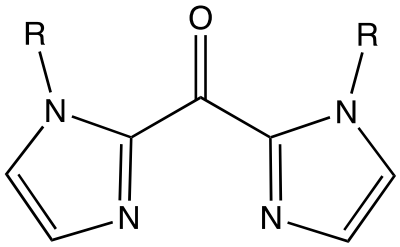

R = methyl, ethyl, vinyl

Scheme 1. Bis(imidazolyl)ketone ligands (^{R}bik).

[a] Sorbonne Université. Institut Parisien de Chimie Moléculaire. UMR CNRS 8232. 4 place Jussieu F-75252 Paris. E-mail : yanling.li@sorbonne-universite.fr
[b] Sorbonne Université. Institut des NanoSciences de Paris. UMR CNRS 7588. 4 place Jussieu F-75252 Paris
[c] "Petru Poni" Institute of Macromolecular Chemistry, Romanian Academy, Aleea Grigore Ghica Vodă 41-A, RO-700487 Iasi, Romania
[d] Coordination and Supramolecular Chemistry Laboratory, "Ilie Murgulescu" Institute of Physical Chemistry, Romanian Academy, Splaiul Independentei 202, Bucharest 060021, Romania
[e] Department of Inorganic Chemistry, Physical Chemistry and Electrochemistry, Faculty of Applied Chemistry and Materials Science, University Politehnica of Bucharest, 1-7 Gh. Polizu Street, 011061 Bucharest, Romania. E-mail: alexandru.gabriela@gmail.com
[f] Departament de Química Inorgànica/Instituto de Ciencia Molecular (ICMol), Universitat de València, C/ Catedrático José Beltrán 2, 46990 Paterna, Valencia, Spain. E-mail: miguel.julve@uv.es

Electronic Supplementary Information (ESI) available: [details of any supplementary information available should be included here]. See DOI: 10.1039/x0xx00000x

only lead to drastic changes in the magnetic properties but also in the optical, dielectric or mechanic properties.[3,11–13] In our group, we have been interested, in the last years, by the design of this last class of magnetic switches by using the bis-imidazolyl-ketone ligands (^{R}bik) shown in the Scheme 1. These ligands actually induce an adequate ligand field at the coordination sphere of the Fe^{II} that makes possible a spin-state change in the FeN_6 chromophore. We have studied for example $[Fe(^{R}bik)_3]^{2+}$ and $[Fe(^{R}bik)_2L_2]$ monometallic complexes in both solution and solid state (L = NCS or NCSe).[14,15] Alternatively, the *N*-donor cyanido-metalloligand can be used to build polymetallic switchable species, such as tetranuclear square complexes, $[Fe(^{R}Tp)(\mu\text{-}CN)]_2[M'(^{R}bik)_2]_2$, where ^{R}Tp is a tris(pyrazo-1-yl)borate ligand and M' = Fe, Co.[16–18] In these cases, when a Co ion occupies the $\{M'(^{R}bik)_2(N\text{-})_2\}$ site, reversible metal-metal electron transfer through the cyanido bridge coupled to a spin transition on the $\{Co(^{R}bik)_2(N\text{-})_2\}$ site can also be responsible for the magnetic bistability.[19,20] We showed for example that the magnetization could be repeatedly switched on and off in a cyanido-bridged Fe_2Co_2 square complex.[21] We also demonstrated that pressure could convert a paramagnetic Fe_2Co_2 complex into a bistable magnetic switch with bistability at room temperature.[22] In the continuation of our work on the use of ^{R}bik ligand to investigate original magnetic properties, we decided to explore the possibility of observing slow magnetic relaxation in Co^{II} based octahedral complexes using the ^{Me}bik as anchoring ligand.

In the last years, the Co^{II} based SIMs have attracted strong interests thanks to the large first order spin-orbital coupling of Co^{II} ion that can lead to significant anisotropy, D. The sign of D and its magnitude depends greatly on the geometry of Co^{II} ion in its first and even secondary spheres of coordination.[23,24] By using various ligands and choosing the coordination numbers of Co^{II} ion from two to eight, it has been possible to obtain a great number of geometries for Co^{II} based complexes: linear, tetrahedral, octahedral, *etc.*[25] Two-coordinated numbers are recognized to favor predominantly uniaxial magnetic anisotropy and allowed achieving the highest *D* value (476.0 cm^{-1}) among all Co^{II} based SIMs.[26] In contrast, the six-coordinate Co^{II} SIMs can lead to either easy-plane ($D > 0$) or easy-axis anisotropy ($D < 0$). Some of us were the first to demonstrate this phenomenon for a distorted octahedral Co^{II} complex, namely *cis*-$[Co^{II}(dmphen)_2(NCS)_2]$ where dmphen = 2,9-dimethyl-1,10-phenanthroline.[27] The systematic magneto-structural study of this family of SIMs is fundamental to understand the effects of various and often combined factors on the magnetic anisotropy and on the relaxation, such as the coordination geometry, the ligand nature and intermolecular interactions, etc. For this reason, the study of six-coordinated Co^{II} based SIMs are now blooming worldwide.[25,28]

In the present work, we describe the preparation and magneto-structural investigation of three new six-coordinate Co^{II} SIMs based on the β-diimine ^{Me}bik ligand: (i) two monometallic $[Co^{II}(^{Me}bik)_2(N\text{-})_2]$ complexes where N is thiocyanate NCS (**1**), and selenocyanate NCSe (**2**); (ii) one mixed-valence $\{Co^{III}_2Co^{II}\}_n$ chain complex (**3**). The latter is composed of $[Co^{II}(^{Me}bik)(H_2O)(dmso)]$ fragments connected to each other by a *N*-donor bimetallic Co^{III}_{LS} cyanido-metalloligand, $(PPh_4)_2[Co_2^{III}(\mu\text{-}2,5\text{-}dpp)(CN)_8]\cdot 2H_2O$ (2,5-dpp = 2,5-bis(2-pyridyl)pyrazine and PPh_4^+ = tetraphenylphosphonium). **1**-**3** display field-induced slow relaxation of magnetization being thus new examples of field-induced SIMs.

Results and discussion

Details of the syntheses and characterization. The mononuclear complexes **1**-**2** are straightforwardly obtained by reacting *in-situ* prepared $[Co^{II}(^{Me}bik)_2(S)_2]^{2+}$ complex (S = solvent) with a stoichiometric amount of NCS^- or $NCSe^-$ salts under ambient conditions, while the chain compound **3** is obtained by reacting $[Co^{II}(^{Me}bik)_2(S)_2]^{2+}$ with the cyanido-bearing dinuclear complex $[Co^{III}_2(\mu\text{-}2,5\text{-}dpp)(CN)_8]^{2-}$. Actually, the reluctance of the dicobalt(III) complex to exchange ligands in solution, its potentially donor terminal cyanide ligands and its overall negative charge make it an very suitable species to be used as a metalloligand toward either fully solvated metal ions or partially blocked metal complexes. This synthetic strategy, which was proved to be successful in previous works,[29] is employed herein to prepare a heterobimetallic $\{Co^{III}_2Co^{II}\}_n$ chain where a bidentate ^{Me}bik ligand is used to partially block the coordination sphere of the cobalt(II) ion. The infrared spectra of **1**-**3** are described in ESI.

Description of the structures. The single crystal X-ray diffraction structures were determined at 200 K (**1** and **2)**, and at 293 K (**3)**. **1**-**2** crystallize in the monoclinic *C*2/c space group, and **3**, in the *Pc* space group. A summary of the crystal data and structure refinement is given in Table 1. Drawings of the structures of the mononuclear $[Co^{II}(^{Me}bik)_2(N\text{-})_2]$ complexes **1**-**2** are shown in Figure 1. No solvent molecules are observed in the crystal lattice of **1**-**2**. Their asymmetric unit is made of half a complex, which is related to the other half through a C_2 symmetry axis. Each Co^{II} ion is in a distorted octahedral coordination environment built by two *cis*-positioned nitrogen atoms from thiocyanate (**1**) or selenocyanate (**2**) and other four nitrogen atoms from two chelating ^{Me}bik molecules. Selected interatomic distances and angles for **1**-**3** are grouped in Table 2. The average values of the Co-N bond lengths with the inorganic and organic ligands amount to 2.111(2) and 2.128(2) Å in **1**, to be compared with 2.118(2) and 2.120(2) Å in **2**. These bond distances are typical for high-spin octahedral Co^{II} complexes and in this respect, they are close to

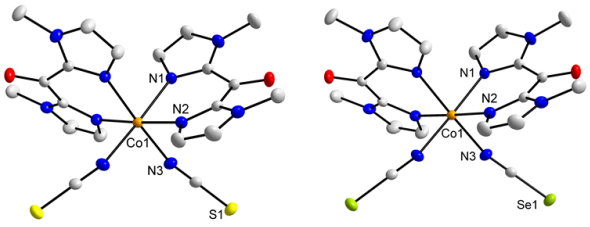

Fig. 1. Perspective views of the mononuclear complexes CoII complexes in the crystal structure of **1** and **2**. The hydrogen atoms are omitted for the sake of clarity. Colour code: Co: orange, N: blue, C: grey, O: red, S: lemon, Se: asparagus.

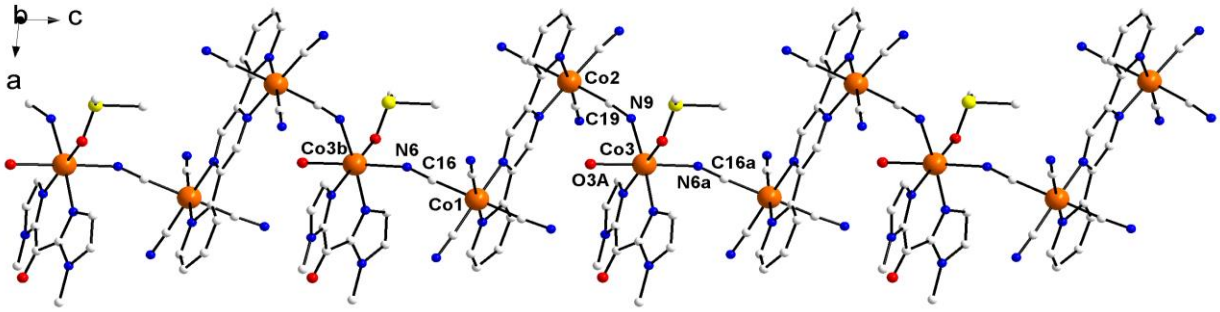

Fig. 2. Perspective view along the crystallographic c axis of a fragment of the mixed valence chain **3** along with the atom numbering of the cyanido bridges and cobalt atoms. The crystallization water molecules and hydrogen atoms are omitted for the sake of clarity. Colour code: Co: orange, N: blue, C: white, O: red, S: lemon.

Table 1. Crystal data and structure refinement for **1**-**3**.

	1	**2**	**3**
Formula	$C_{20}H_{20}CoN_{10}O_2S_2$	$C_{20}H_{20}CoN_{10}O_2Se_2$	$C_{33}H_{30.80}Co_3N_{16}O_{4.40}S$
Crystal system	Monoclinic	Monoclinic	Monoclinic
Space group	C2/c (15)	C2/c (15)	Pc
a/Å	7.5868(3)	7.7139(3)	12.231(3)
b/Å	14.4413(7)	14.5798(5)	8.1876(11)
c/Å	22.1581(8)	22.4322(7)	21.110(4)
α/°	90	90	90
β/°	99.377(2)	99.092(2)	96.09(2)
γ/°	90	90	90
V/Å^3	2395.27	2491.19(15)	2102.0(7)
Z	4	4	2
Dc/g cm $^{-3}$	1.540	1.731	1.471
T/K	200	200	293(2)
Radiation (Å)	CuKα (λ = 1.54178)	CuKα (λ = 1.54178)	MoKα (λ = 0.71073)
μ/mm^{-1}	7.596	9.080	1.277
F(000)	1140	1284	946
Refl. Collected	9312	7437	14566
Refl. indep. [R(int)]	2110 [0.0355]	2245 [0.0266]	6888 [0.1124]
Data/restraints/param.	2110/0 161	2245/0/161	6888 / 38 / 531
Goodness-of-fit on F^2 (S)[c]	1.065	1.047	1.012
Final R indices [I >2σ(I)]R_1[a].	0.0277	0.0266	0.0869.
wR_2 [b]	0.0756	0.0671	0.1326
R indices (all data) R_1[a].	0.0288	0.0292	0.1665.
wR_2 [b]	0.0764	0.0684	0.1638
Δρmax.min/ e Å^{-3}	0.24 / -0.17	0.37 / -0.38	0.610 / -0.475
CCDC deposition number	2096752	2096753	2072597

[a]$R_1 = \sum||F_o| - |F_c||/\sum|F_o|$. [b]$wR_2 = \{[\sum w(F_o^2 - F_c^2)^2/\sum w(F_o^2)^2]\}^{1/2}$, $w = 1/[\sigma^2(F_o)^2 + (mP)^2]$ with $P = (F_o^2 + 2F_c^2)/3$. m = 0.0399 (x). [c]$S = [\sum w(|F_o| - |F_c|)^2/(N_o - N_p)]^{1/2}$.

those previously reported for the parent high-spin $[Co(^{Me}bik)_3](BF_4)_2$ complex.[20] The distortion from the octahedral geometry of the Co^{II} environment can be estimated by measuring the sum of the deviation from orthogonality of the twelve pseudo-orthogonal N-Co-N angles involving the set of nitrogen donor atoms (ΣCo). The measured values of ΣCo are 32.99° (**1**), 33.02° (**2**) and 27.90° (**3**) respectively. They are all similar to that measured in related photo-induced high-spin $[Co^{II}(^{Me}bik)(N\text{-})_2]$ complex (41.0°).[21] The distortions of the Co^{II} coordination sphere were also analysed by continuous shape measurements using the SHAPE 2.1 program.[31] The reported output, SHAPE factor OC-6, allows assessing the matching between an idealized polyhedron and the actual coordination sphere: the lower the shape factor is,

Table 2. Selected bond length and angles for **1**-**3**.

Bond length (Å) /Angle (°)	**1**	**2**	**3**
Co1-N1(^{Me}bik)	2.1257(14)	2.1187(19)	
Co-N2 (^{Me}bik)	2.1283(15)	2.1199(19)	
Co-N3 (^{a}L)	2.1113(15)	2.1180(2)	
Co3-N13(^{Me}bik)			2.119(15)
Co3-N14(^{Me}bik))			2.100(16)
Co3-N6a (CN)			2.137(17)
Co3-N9 (bridging CN)			2.143(18)
Co3-OA (water)			2.149(11)
Co3-O2 (DMSO)			2.074(13)
Σ Co^{II} (°)	32.99	33.02	27.9
∠Co^{II}CO (°)	164..88(12)	165.41(16)	167.4
∠Co^{II}NCX (°)	159.79(15)	160.2(2)	155.5
∠Co3NC(Bridging CN) (°)			147.5
∠dihedral imidazoles (°)	22.75(14)	21.19(13)	19.73

^{a}L = NCS (**1**), NCSe (**2**) and CN (**3**).

the better the matching between the actual coordination sphere and the idealized polyhedron. The analyses led to numerical values of 0.171 (**1**), 0.169 (**2**) respectively for OC-6 (zero would correspond to an ideal octahedron). These values indicate a small distortion and they are smaller than that value observed in the high-spin $[Co^{II}(^{Me}bik)_3](BF_4)_2$ complex (0.420). Concerning the geometry of the ligands, the bidentate β-diimine ^{Me}bik ligands are not planar, although the presence of the C=O group between the two imidazolyl groups confers some aromaticity to the ligand and thus, a π-acceptor character.[15] Here the dihedral angles between the imidazolyl rings are 22.84 (**1**), 21.26 (**2**) at 200K and 22.24° (**3**) at 293 K. The NCX ligands (X = S or Se) in **1** and **2** are almost linear (178.61 and 178.62°, respectively), however the Co-N-C angles deviate~~s~~ significantly from linearity [*ca.* 159.87 (**1**) and 160.34° (**2**)], as previously observed in related $[Fe(^{Me}bik)_2(NCX)_2]$ spin-crossover complexes.[14] The compounds **1** and **2** are isomorphous. Omitting the short contacts implying the hydrogen atoms, the short contacts [ca. 3.320 (**1**) and 3.353 Å (**2**)] between the S/Se atoms and the C atom from the carbonyl group at ^{Me}bik ligand form a supramolecular 2D motif (see ESI). The short contacts [ca. 3.088 (**1**) and 3.150 Å (**2**)] between the electron-poor C atom (methyl group) and electron rich O atom (C=O group) from two ^{Me}bik ligands belonging to two neighbouring layers contribute to the cohesion between layers (see ESI). The shortest Co···Co distances within each supramolecular layer are 8.16 and 8.25 Å for **1** and **2** respectively, whereas the corresponding shortest Co···Co distances between two neighbouring layers are somewhat longer [11.12 (**1**), 11.28 (**2**) Å].

The structure of **3** consists of neutral zig**-**zag chains of formula $[Co^{II}(^{Me}bik)(H_2O)(dmso)(\mu\text{-}NC)_2Co_2^{III}(\mu\text{-}2,5\text{-}dpp)(CN)_6]_n{\cdot}1.4nH_2O$ whose asymmetric unit is made up of a $\{Co^{II}(^{Me}bik)(H_2O)(dmso)\}^{2+}$ fragment coordinated to a $\{Co^{III}_2(\mu\text{-}2,5\text{-}dpp)(CN)_8\}^{2-}$ metalloligand. This dicobalt(III) unit connects further, through a cyanido group, to another cobalt(II) entity in a pseudo *trans* arrangement, building a mixed valence $\{Co^{III}_2Co^{II}\}_n$ chain, which runs along the crystallographic *c* axis. The two cobalt atoms from the dicobalt(III) fragment (Co1 and Co2) are six-coordinated, two nitrogen atoms belonging to the bridging 2,5-dpp ligand and four cyanide-carbon atoms building somewhat distorted octahedral geometries around them. The values of the bite angle subtended by the bridging 2,5-dpp ligand at Co1 and Co2 are 83.7(6) and 81.7(6)°, respectively. The Co-$C_{cyanido}$ bond distances cover the ranges 1.84(2)-1.88(2) (at Co1) and 1.88(2)-1.97(2) Å (at Co2), these values being shorter than the Co-$N_{2,5\text{-}dpp}$ bond lengths [1.952(14) and 1.970(3) Å at Co1 and 1.984(14) and 1.999(14) Å at Co2]. The Co-C-$N_{cyanide}$ angles are close to linearity [values in the ranges 173.7(7)-177(2) (Co1) and 172.2(16)-178.2(17)° (Co2)] (ESI). The Co1···Co2 separation across the bridging 2,5-dpp molecule is 6.66 Å. The values of the structural parameters for this dicobalt(III) fragment agree with those previously reported for the related chains of general formula $[M^{II}(CH_3OH)_2(dmso)_2(\mu\text{-}NC)_2Co_2^{III}(\mu\text{-}2,5\text{-}dpp)(CN)_6]_n{\cdot}4nCH_3OH$ (M = Co and Fe).[29] Each $\{Co^{II}(^{Me}bik)(H_2O)(dmso)\}$ node contains six-coordinate cobalt(II) ions (Co3) in an almost ideal octahedral geometry as estimated by the *SHAPE 2.1* program (0.160 for OC-6).[30] The valence of the Cobalt ions was confirmed by using the Bond Valence Sum model (see ESI). The equatorial plane is formed by two nitrogen atoms from a chelating ^{Me}bik molecule [2.119(15) and 2.100(16) Å for Co3-N13 and Co-N14, respectively; the value of the bite angle, N13-Co3-N14, being 84.3(6)°, one dmso-oxygen atom [2.074(13) Å for Co3-O2], and one bridging cyanide-nitrogen atom [Co3-N9 = 2.143(18) Å]. The axial positions at Co3 (ESI) are filled by one water molecule (O3A) and a cyanide-nitrogen atom (N6a) with Co3-O3A and Co3-N6a bond lengths of 2.149(11) and 2.137(17) Å, respectively. The cyanido bridges at the cobalt(II) side are quite bent, [angles of 147.5(15) and 155.5(18)° for Co3-N9-C19 and Co3-N6a-C16a, respectively] and the values of the cobalt···cobalt separation across the single cyanide bridges are ca. 4.92 (Co3···Co2) and 5.03 Å (Co3···Co1). The shortest interchain cobalt···cobalt distance is 8.61 Å for Co2···Co1n Å [symmetry code (n) = -1+*x*, *y*, *z*]. An extensive network of intra- and interchain hydrogen bonds involving the coordinated and free water molecules and terminal cyanide-nitrogen atoms [O4W···O1W, OA···N11m, O4W···N7n and O4W···N10m] leads a supramolecular 3D framework and contributes to the stabilization of the structure (see ESI).

***Ab-initio* calculations of zero-field splitting (ZFS) parameters D and E.** The parameters *D* and *E*, which define the axial and rhombic components of the ZFS, depend directly on the electronic structure; that is, both on the electronic distribution of the ground state and the energies of excited states that interact with the former through spin-orbit coupling. Summarizing, the molecular geometry and the strength of the ligand field will account for these parameters. The value of the *E*/*D* ratio, which takes values between 0 and 1/3, should be directly related to the symmetry of the crystal-field, mainly to its rhombic distortion. The geometry of the coordination sphere, its distortion, the electronic nature of the different ligands that make it up, and their orientation relative to a metal-ligand bond in the case of

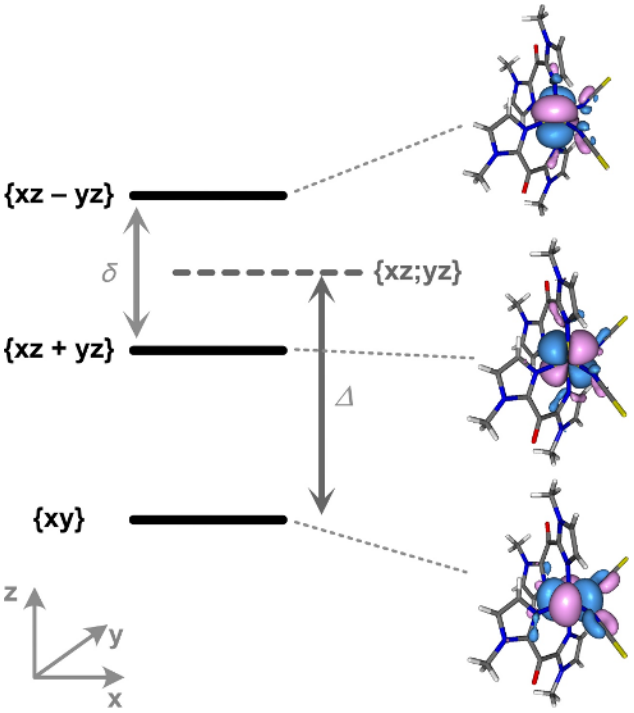

Fig 3. Splitting of the term energies obtained from a CASSCF/NEVPT2 calculation on the experimental geometries of 1 and 2. The notation of the three states coming from the $^4T_{1g}$ term in Oh symmetry was done with the only half-filled T_{1g} orbital.

pseudohalides influence *D* and *E*/*D*. For this reason, understanding the found sequences of *D* and mainly of *E*/*D* ratio in this family of compounds can be an arduous task. Theoretical calculations, which provide ZFS parameters and energies of the states contributing to them, can help to rationalize the experimental results for **1**-**3**.

High-spin d^7 octahedral cobalt(II) complexes exhibit two filled t_{2g} orbitals in their ground state. Additionally, one t_{2g} and two e_g orbitals are half-filled being thus magnetic orbitals. Promoting a β electron from the two filled t_{2g} orbitals to the remaining t_{2g} orbital leads to the two closest excited states. These excited states, which largely mix with the ground one through a SOC and providing the most significant contributions (D_i) to *D*. These three states, excited and ground ones, constitute the $^4T_{1g}$ term in an ideal O_h symmetry. The loss of symmetry in the crystal field by axial compression or elongation causes its splitting in the ^4E and ^4A states. The loss of symmetry in the equatorial ligand-field by a rhombic distortion induces a subsequent splitting of the ^4E state. All these distortions together lead to the three above-mentioned near states, which will now be labelled with the half-filled orbital, {*i*}. Our calculations show that **1**-**2** exhibit a similar electronic configuration with a half-filled *xy* orbital for the ground state. For simplicity, two imidazole groups in *trans* positions and coming from different ^{Me}*bik* ligands define the z-axis of the coordination octahedron. The two remaining imidazole groups and two pseudohalides constitute the equatorial plane. In this way, the ground and two closest excited states are labelled as {*xy*}, {*xz* + *yz*}, and {*xz* – *yz*}, respectively, being the last ones a combination of orbitals that places the resulting orbital at the interbond spaces. However, drawing similar conclusions in **3** is more complicated. According to molecular orbitals, the z-axis should be close to the axis formed by the metal center and the nitrogen and oxygen atoms from the coordinated imidazole group and water molecules. However, the orientation of the ZFS tensor shows the *z*-axis partially offset and not pointing to any metal-ligand bonding direction (ESI). This fact conducts to a {*xz* + *yz*} state as ground state, making difficult discussing together the results for **1**-**3**. Imidazole, pseudohalide, dmso and water groups show a different intensity in their ligand-field and, therefore, a splitting of the $^4T_{1g}$ term. Being the ligand field for the pseudohalides weaker than that for imidazole group, as its strength is intensified advancing throughout the NCS^-, $NCSe^-$ series, the ligand-field will be more symmetric, the excited states closer to the ground one and the D_i contributions more significant. Coordinated water and dimethylsulphoxide molecules exhibit a weaker ligand-field and causing therefore the low energy of the two excited states and the largest D_i contributions. Both theoretical global values of *D* (table 3) and D_i contributions from the excited states as a function of their energies support these conclusions. According to a 2nd-order perturbation theory, when these energies are large enough, D_i is a function of $1/E_i^2$, as it occurs for most of our results. However, the lower-lying {*xz* + *yz*} excited state for **3** is very stable. In such a case, a 1st-order SOC approach is more appropriate. Strangely, D_i for all data follows a linear dependence with E_i (see ESI).

The splitting of the ^4E state induced by an asymmetry of the electronic density in the equatorial plane causes a rhombicity in the ZFS; the *E*/*D* ratio stops being null. Equatorial distortions can cause this loss of symmetry, but this is not the case, as the shape measures for **1**-**3** show, instead, the presence of ligands of different electronic nature causes it. According to Figure 3, Δ and δ define the average energy of the excited states and the energy gap for the last ones. Δ accounts for the axial anisotropy and δ, actually δ/Δ quotient, for the rhombic anisotropy expressed by the *E*/*D* ratio. According to this, the magnitude of δ/Δ for **1** (0.38) and **2** (0.50), which show a similar electronic interpretation, agrees with their calculated *E*/*D* ratio.

Table 3. Values of E/D, D, g_1, g_2 and g_3 for **1**-**3** determined by DFT calculations

	1	**2**	**3**
E/D	0.090	0.120	0.078
D (cm^{-1})	89.90	93.90	127.20
g_1	6.07	7.00	5.16
g_2	4.49	4.30	3.62
g_3	2.50	2.45	2.21

EPR spectroscopy and magnetic measurements. X-band (**1**-**2**) and the Q-band EPR spectra (**3**) on powdered samples at 4.0 K are depicted in Figure 4. These spectra are characteristic of octahedral high-spin Co^{II} complexes with rhombic symmetry and large zero-field splitting ($D \geq E/3 >> 9.34$ GHz). The three signals related to the g_1, g_2 and g_3 components of the effective *g* tensor are very broad. This is probably because of the unresolved

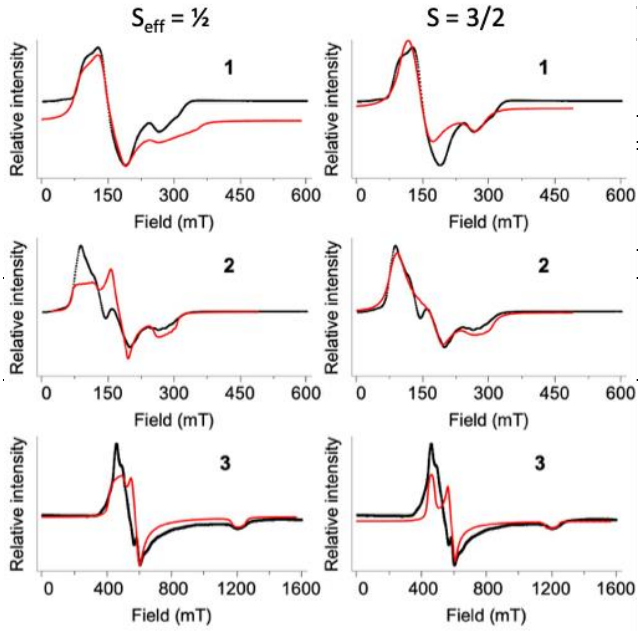

Fig. 4. Experimental (black) and simulated (red) powder X-band EPR spectra for 1-2 and powder Q-band for **3** at 4.0 K. The simulations have been carried out using an effective spin S_{eff} = ½ (left column) and an anisotropic spin S = 3/2 with E/D ratio obtained from *ab-initio* calculations (right column).

Table 4. Values of the *g* factor and hyperfine constants resulting from the simulation of the EPR spectra through the anisotropic *S* = 3/2 model for **1**-**3**

	g factor			Hyperfine constants (MHz)			distortion of Co^{II}	
	g_1	g_2	g_3	A_1	A_2	A_3	ΣCo	Shape F. OC-6
1	2.55	2.54	2.48	200	200	120	32.99	0.171
2	2.52	2.47	2.41	440	440	250	33.02	0.169
3	2.40	2.38	2.07	180	180	320	27.90	0.160

hyperfine interaction with the *I* = 7/2 cobalt nucleus. The intensity of all spectra increases with the decreasing temperature (see ESI section for **3**), indicating unambiguously that *D* is of positive sign and the effective spin value of the fundamental ground state is ½ for the three compounds. So, considering a S_{eff} = ½, the simulation of the EPR spectra of **1**-**3** was achieved with the following g_1. g_2 and g_3 parameters: 5.40, 3.25 and 1.75 (**1**), 6.20, 4.15 and 2.15 (**2**) and 5.30, 4.25 and 2.01 (**3**). These sets of values agrees with a positive sign of the *D* parameter in them after the Bencini's study on EPR spectroscopy of cobalt(II) complexes,[31] such as those obtained through the numerical simulation of the EPR spectra through a S = 3/2 model and the simultaneous fit of the magnetic susceptibility and magnetization data (see below). with S = 3/2 by using the Easyspin program[32], the simulation of EPR spectra was achieved only with *D* > 0 and small values of the *E/D* quotient. As the simulated EPR spectra don't change significantly with small variation of E/D ratio, the E/D values determined from *ab-initio* calculations were used. The experimental values of g parameters confirm the positive D values for the three compounds. The simulated plots for the S_{eff} = ½ and *S* = 3/2 models follow roughly well the experimental curves as shown in Figure 4. The large values of *D* and the slight deviations of the octahedral geometry of **1**-**3** account for the small values of the *E/D* quotient along this series of compounds (0.078-0.120)(Table 3).

In order to further probe the electronic states of metal ions in the three compounds, magnetic susceptibility measurements in DC mode were performed in the temperature range of 2-300 K and the magnetization was measured at different fields between 2.0 and 8 K. The $\chi_M T$ *versus T* curves for **1**-**3** are shown in Figure 5, the inserts being the corresponding reduced magnetization plots (χ_M is the molar magnetic susceptibility, *T* is the temperature and *H* is the applied dc magnetic field). At room temperature, the values of $\chi_M T$ are 2.94. 3.06 and 2.93 $cm^3\ mol^{-1}K$ for **1**-**3**, respectively. These values fall in the expected range of 2.7-3.2 $cm^3\ mol^{-1}\ K$ for a six-coordinate high-spin cobalt(II) ion with a significant orbital momentum. Upon cooling, the $\chi_M T$ value decreases gradually between 300-100 K and then drastically below 100 K to reach 1.72, 1.73 and 1.56 $cm^3\ mol^{-1}\ K$ at 2 K for **1**-**3**. This decrease of $\chi_M T$

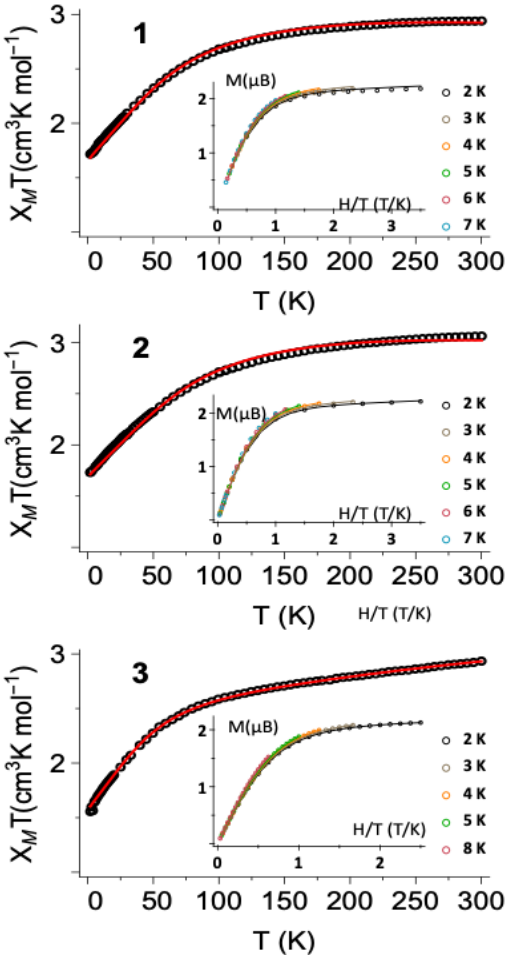

Fig. 5. Experimental and fitted simulated $\chi_M T$ product against the temperature for **1**–**3**. The inserts show the reduced magnetization plots for each compound at the quoted temperatures.

is due to the thermal depopulation of the higher energy Kramer's doublets of the Co^{II}_{HS} centre and/or antiferromagnetic interactions between these paramagnetic units. However, this

last possibility is ruled out because the large values of the shortest intermolecular [8.17 (**1**), 8.25 (**2**) and 12.23 Å (**3**)] and intrachain [10.57Å (**3**)] cobalt(II)-cobalt(II) separation. The saturation magnetization values at 2.0 K are 2.18, 2.22 and 2.11 μB for **1**-**3**. The reduced magnetization curves quasi collapse, indicating large *D* values and irrelevant changes in the thermal depopulation of the higher energy Kramer doublets below 8.0 K.[33,34] The temperature and field dependent magnetic data were analyzed simultaneously by using the PHI program,[35] with the spin Hamiltonian described by eq (1).

$$\mathbf{H} = D\,[\mathbf{S_z^2} + S(S+1)/3)] + E\,(\mathbf{S}_x^2 + \mathbf{S}_y^2) + \mu_B g \mathbf{BS} \qquad (1)$$

where *D*, *E*, μ_B and *g* are the axial and rhombic ZFS parameters, the Bohr magneton and *g* parameter, respectively. **S** and **B** represent the spin operator, and the magnetic field vector. The TIP (temperature independent paramagnetism) was implied in the simultaneous simulation of $\chi_M T$ *vs T* and *M vs H/T*. Again, the fitted $\chi_M T$ *vs T* and *M vs H/T* curves don't show any sensitive variation with the small *E/D* ratio, the range of the *E* parameter was chosen by taking into consideration of the *E/D* ratio obtained

Table 5. Hamiltonian parameters resulting from the simultaneous simulation of $X_M T$ vs *T* and *M* vs *H* data for **1**-**3**.

		Anisotropy			TIP	Residual
	g	*D* (cm^{-1})	*E* (cm^{-1})	*E/D*	X10^3	X10^3
1	2.4355	59.84	5.20	0.087	0.813	4.976
2	2.4721	66.32	8.00	0.121	0.911	1.375
3	3.0188	70.49	6.00	0.085	0.633	1.248

by *ab-initio* calculations. An isotropic g factor was used for the fitting to limit the fitted parameters. The quality of the fit *q* is given by the "residual" parameter defined as $[\Sigma(P_{exp}-P_{calc})^2]/[\Sigma(P_{exp}-P_{calc})^2]$[36] where P is the physical property under study ($\chi_M T$ and *M)*. All these parameters for **1**-**3** are summarized in Table 5. The theoretical values *of* $\chi_M T$ and *M* values for all three compounds agree with the experimental ones (see Figure 5), as reflected by the small residual values. The values of the *D* parameter are 59.84, 66.32 and 70.49 cm^{-1} for **1**, **2** and **3** respectively. They are smaller than that obtained by *ab-initio* calculations [89.90 (**1**), 93.90 (**2**) and 127.20 (**3**) cm^{-1}]. The lower concordance between the experimental and theoretical *D* values for **3**, the former being too small, was already observed in the past in other compounds[23] that, like **3**, present labile coordinated solvent molecules.

Finally, the dynamic magnetic properties of **1**-**3** were probed by measuring the alternating current (ac) magnetic susceptibility. The out-of-phase susceptibility (χ_M'') does not show any frequency dependence in the lack of an applied dc field. This is not surprising considering that the important transversal anisotropy of the four compounds can cancel the slow relaxation of magnetization through quantum tunneling of the magnetization (QTM) at zero field. When suppressing the QTM effect by the application of a suitable static field (0.16, 0.17 and 0.10 T for **1**, **2** and **3**, respectively), χ_M' and χ_M'' become frequency dependent. This behaviour is typical of the field-induced SIMs.

The dc field for each compound was the field corresponding to the peak value of the out-of-phase magnetic moment *M*'', when recording *M*'' under various fields from 0 to 5000 Oe at 2.5 K. Figure 6 illustrates the Cole-Cole plot for **2** and the corresponding χ_M'' versus frequency in logarithmic scale at temperatures in the range 2.5 to 8 K. The Cole-Cole and χ''_M plots for **1** and **3** are in the ESI section. The ac magnetic susceptibility data have been fitted into a generalized Debye model using a home-made Mathematica® program and according to a two-step procedure described in a previous work.[37] The parameters extracted from the analysis of the ac data are listed in Tables S3-S6 in ESI, where χ_S and χ_T are the minimum and maximum values of χ_M' when the χ_M'' versus χ_M' curves cross the χ_M' axis, α is a parameter indicating the deviation degree of the relaxation from the ideal Debye process, and τ is the relaxation time.

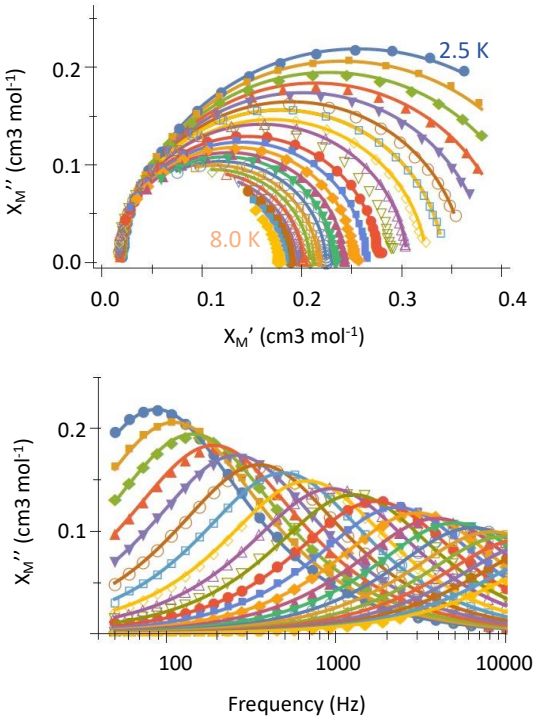

Fig.6. Cole-Cole plot (top) and χ_M'' against frequency in logarithmic scale (bottom) for **2**, the solid lines are the best fits of the data to a generalized Debye model.

Generally, the relaxation of Co^{II} based SIMs is the addition of four processes described by the eq. (2)[38]

$$\tau^{-1} = B_1/(1 + B_2H^2) + AT + CT^n + \tau_0^{-1}\exp(-U_{eff}/k_BT) \qquad (2)$$

which correspond to the QTM, one-phonon direct relaxation at low temperatures, multi-phonons Raman relaxation and high temperature Orbach relaxation at high temperatures. Each process is characterized by various constants: B_1 and B_2 are for QTM; *A* is for direct relaxation; *C* and *n* are for Raman process; U_{eff} is the magnetic anisotropy barrier and τ_0, the intrinsic relaxation time; k_B is the Boltzmann constant and *H* is the *applied* magnetic field. According to our experience, the QTM effect becomes insignificant under an optimized dc field. As the Orbach process is ruled out for Co^{II} based SIMs with $D > 0$,[29] the relaxation

of the magnetization in **1**–**3** is therefore a combination of direct and Raman processes, as described by eq (3):

$$\tau^{-1} = AT + CT^{n} \qquad (3)$$

Figure 7 shows the experimental and simulated τ^{-1} versus *T* curves for **1**-**3** through eq (2) and the Table 6 summarizes the best-fit values values of the *A*, *C* and *n* parameters. The *n* parameter varies from 6.047 to 6.821 for **1**–**3**, values which fall within the range of 6-8 considered reasonable for Raman relaxation.[29]

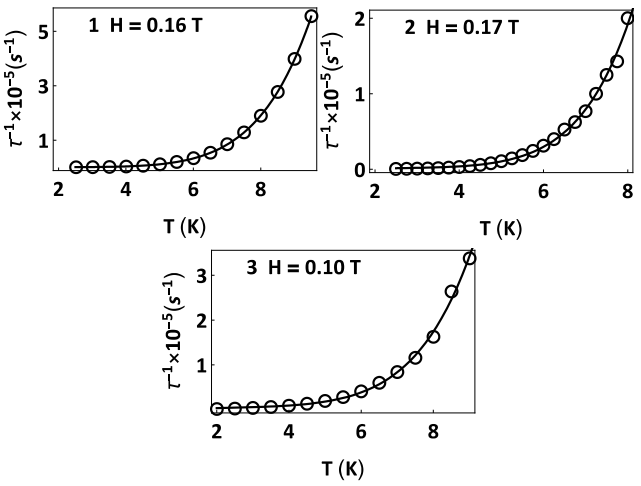

Fig. 7. Experimental and calculated τ-1 versus T curves for **1**-**3** through a combination of direct and Raman approaches.

Table 6. Values of the best-fit parameters for direct and Raman relaxations in **1**-**3**

	A (s^{-1})	*C* ($s^{-1}\cdot K^{-n}$)	*n*	DC field (T)
1	279.34	0.4208	6.257	0.16
2	575.21	0.1295	6.821	0.17
3	1692.95	0.5548	6.047	0.10

Experimental

Materials and Synthetic procedures. All reagents and solvents were purchased from commercial suppliers and used without further purification. The ^{Me}bik, and 2,5-dpp molecules and the $(PPh_4)_2[Co_2^{III}(\mu\text{-}2,5\text{-dpp})(CN)_8]\cdot 2H_2O$ metalloligand were prepared according to the literature.[39] $[Co(^{Me}bik)_2(CH_3CN)_2][BF_4]_2$ was synthesized by in situ reaction of $Co(BF_4)_2\cdot 6H_2O$ (40 mg, 0.12 mmol) and ^{Me}bik (45 mg, 0.23 mmol) in an acetonitrile/water (4:1 v/v, 10 mL) solvent mixture.[20] Elemental analyses (C, H, N) were performed with a Perkin-Elmer 240C analyser at the ISCN (Gif sur Yvette. France). FTIR spectroscopic data were measured on a Vertex 70 Bruker instrument and collected in the 400-4000 cm^{-1} range at room temperature (with a 4 cm^{-1} resolution), in ATR (**1** and **2**) and transmission (**3**) modes.

Synthesis of $[Co^{II}(^{Me}bik)_2(NCS)_2]$ (1) and $[Co^{II}(^{Me}bik)_2(NCS)_2]$ (2). To a methanolic stirred solution solution (40 mL) of ^{Me}bik (0.8 mmol) was added 15 ml solution of $Co(BF_4)_2.6H_2O$ (0.4 mmol) in the same solvent. To the resulting pale/yellow solution, 7 ml methanolic solution of KNCS or KNCSe (0.8 mmol) was added dropwise, pale yellow precipitates were formed. The mixture was stirred 30 minutes and the yellow precipitates were filtered, dried in air and recrystallized in hot DMF (40-50 ml). After 3-4 days at 50°C, nice single crystals suitable for X-ray diffraction were obtained. Yield: 81 (**1**) and 86% (**2**). IR (ATR): (**1**) ν_{max}/cm^{-1}: 3147, 3127, 2959, 2100 (NC_{NCS}), 2066 (NC_{NCS}), 1639 (CO_{bik}), 1520, 1484, 1417, 1170 cm^{-1}. (**2**) ν_{max}/cm^{-1}: 3144, 2953, 2097 (NC_{NCSe}), 2069 (NC_{NCSe}), 1628 (CO_{bik}), 1518, 1482, 1416, 1288, 1170, 892 cm^{-1}. Anal. Calcd for $C_{20}H_{20}CoN_{10}O_2S_2$ (**1**): C. 43.24; H. 3.63; N. 25.21. Found: C. 42.96; H. 3.66; N. 24.80%. Anal. Calcd for $C_{20}H_{20}CoN_{10}O_2Se_2$ (**2**): C. 37.00; H. 3.10; N. 21.57. Found: C. 36.86; H. 3.16; N. 21.30%.

Synthesis of $[Co^{II}(^{Me}bik)(H_2O)(dmso)(\mu\text{-}NC)_2Co_2^{III}(\mu\text{-}2.5\text{-dpp})(CN)_6]_n\cdot 1.4nH_2O$ (3). A water/acetonitrile solution containing the $[Co(^{Me}bik)_2(CH_3CN)_2][BF_4]_2$ complex was layered over a dmso solution (5 mL) of $(PPh_4)_2[Co_2^{III}(\mu\text{-}2.5\text{-dpp})(CN)_8]\cdot 2H_2O$ (76 mg. 0.06 mmol) in a test tube. X-ray quality pale orange prisms of **3** were grown after three weeks under ambient conditions. Yield: ca. 65%. Anal. calcd. for $C_{33}H_{30.80}Co_3N_{16}O_{4.40}S$ (4): C, 42.54; H, 3.31; N, 24.06. Found: C, 42.49; H, 3.27; N, 24.04%. IR (KBr)ν_{max}/cm^{-1}: 3490(s.br), 2923(w), 2185(m), 2142(s), 1630(m), 1605(m), 1513m, 1486w, 1467(m), 1441(m), 1418(vs), 1370(s), 1292w, 1195(s), 1004(m), 900(s), 784(s), 425(m).

X-ray crystallography. Single crystals of **1** and **2** were selected. mounted onto a cryoloop. and transferred in a cold nitrogen gas stream. Intensity data were collected with a BRUKER Kappa-APEXII diffractometer with micro-focused Cu-Kα radiation (λ=1.54178 Å). Data collection were performed with APEX2 suite (BRUKER). Unit-cell parameters refinement, integration and data reduction were carried out with SAINT program (BRUKER). SADABS (BRUKER) was used for scaling and multi-scan absorption corrections. In the WinGX suite,[40] the structures were solved with SHELXT-144 program and refined by full-matrix least-squares methods using SHELXL-14.[41]

Diffraction data of a single crystal of **3** were measured on an Oxford Diffraction XCALIBUR E CCD diffractometer equipped with graphite-monochromated Mo-Kα radiation (λ = 0.71073 Å). The crystals were positioned 40 mm from the CCD detector. The determination of the unit cell and data integration were performed by using the CrysAlis package of Oxford Diffraction.[43] The structure was solved by direct methods by means of the Olex2 software[40,44] with the SHELXS-2014 structure solution program and refined by full-matrix least-squares on F^2 with SHELXL-2014[42] with anisotropic displacement parameters for the non-hydrogen atoms. All hydrogen atoms attached to carbon were introduced in idealized positions ($d_{C\text{-}H}$ = 0.96 Å) using the riding model with their isotropic displacement parameters fixed at 120% of the riding atom. The structural images were obtained with the Diamond 4 program[45] The unit cell parameters and refinement conditions for **3** are given in Table 1 whereas selected bond lengths and angles are listed in Table 2.

CCDC 2096752, 2096753 and 2072597 contain the supplementary crystallographic data for this paper. The data can be obtained free of charge from The Cambridge Crystallographic Data Centre via www.ccdc.cam.ac.uk/structures

Powder X-ray diffraction (XPRD) measurements were done on a PANalytical Empyrean X-ray diffractometer using Cu-Kα radiation (λ = 1.5418 Å) in which the X-ray tube was operated at 40 kV and 30 mA from 5 to 30° (see ESI).

Magnetic measurements and EPR spectroscopy. Direct current (dc) magnetic susceptibility measurements (2.0-300 K) under applied dc magnetic fields of 5000 G (T ≥ 50 K) and 250 G (1.9 ≤ T ≤ 50) and variable-field [0-7 (**1** and **2**) 0-5 T (**3**)] magnetization measurements (2.0-10 K) on crushed crystals (mixed with grease to avoid the crystallite orientation) were carried out with two Quantum Design SQUID magnetometers (MPMS-XL7 and MPMS-XL5). Variable-temperature (2.0-12 K) alternating current (ac) magnetic susceptibility measurements under different applied dc magnetic fields in the range 0-1700 G were performed for **1**-**3** by using a Quantum Design Physical Property Measurement System (PPMS). The magnetic susceptibility data of **1**-**3** were corrected for the diamagnetism of the constituent atoms and the sample holder (a plastic bag). X-band EPR spectra for **1**-**2** and Q-band EPR spectra for **3** at 4.0 K (4.0-20 K for 4) on powdered samples were registered with two Bruker ER 200 spectrometers equipped with a helium continuous-flow cryostat. The EPR spectra were fitted through the version 5.2 of the EasySpin software.[34]

Computational studies. The parameters that determine the axial (*D*) and rhombic (*E*) components of the local zero-field splitting (ZFS) of **1** and 2 were estimated from theoretical calculations based on Complete Active Space theory (CASSCF), which often provides accurate values of the nearby excited states energies and for the ZFS tensor of mononuclear first-row transition metal complexes. Calculations were carried out on the experimental geometries with version 4.0 of the ORCA programme[46] using the def2-TZVP basis set proposed by Ahlrichs[47,48] and the auxiliary TZV/C Coulomb fitting basis sets.[49-51] The contributions to ZFS from 10 quartet and 20 doublet excited states generated from an active space with seven electrons in five d orbitals were included using an effective Hamiltonian. RIJCOSX method was used combining resolution of the identity (RI) and "chain of spheres" COSX approximations for the Coulomb and exchange terms, respectively.[52,53]

Conclusions

In summary, the coordination of Co^{II} ion by ^{Me}bik ligand can give six-coordinate mononuclear complexes (**1**-**2**) or a 1D chain (**3**), which exihibit field-induced SIM behaviours. The Co^{II} ion in **3** has a CoN_4O_2 environment with nearly ideal octahedral geometry, while in $Co(^{Me}bik)_2(L)_2$ with L = NCS (**1**) and NCSe (**2**), the Co^{II} ion is in a slightly more distorted CoN_6 surrounding. All the three compounds display $D > 0$ and a rhombicity which increases with the distortion of the Co^{II} coordination sphere. The slow relaxation of the three compounds can be described by the combination of direct and Raman processes.

Conflicts of interest

There are no conflicts to declare.

Author Contributions

M.-G.A., D.V., J.-R. J., H. S. and B.Q. X prepared the complexes and grew the single crystal and analyze the FTIR spectra - Investigation; L.-M C. and S.S. carried out the X-ray diffraction experiments - Investigation; J.V. B performed EPR spectra measurements – Investigation; Y.L. performed the magnetic measurements and analyzed EPR and magnetic data - Investigation; J.C. carried out the theoretical calculations and discussed their results – Formal analysis; M.J., R.L., M.-G.A. and Y. L. conceived and designed the experiments – Conceptualization and Methodology; all authors contribute to the writing of the manuscript, and all agree in the decision to publish the results.

Acknowledgements

Financial support from Sorbonne Université, CNRS, the Ministère de l'Education et de la Recherche, Ministry of Research, Innovation and Digitization, CNCS/CCCDI – UEFISCDI (project PN-III-P1-1.1-TE-2019-0352), the Spanish MICIU (Project PDI2019-109735GBI00 and Unidad de Excelencia Maria de Maetzu CEX2019-000919-M) is gratefully acknowledged.

Notes and references

1 R. Winpenny and G. Aromí, Eds., *Single-molecule magnets and related phenomena*, Springer, Berlin, 2006.
2 O. Kahn, *Molecular magnetism*, Wiley-VCH, New York, 2001.
3 M. A. Halcrow, Ed., *Spin-crossover materials: properties and applications*, Wiley, Chichester, 2013.
4 R. Sessoli, D. Gatteschi, A. Caneschi and M. A. Novak, *Nature*, 1993, **365**, 141–143.
5 R. Lescouëzec, L. M. Toma, J. Vaissermann, M. Verdaguer, F. S. Delgado, C. Ruiz-Pérez, F. Lloret and M. Julve, *Coord. Chem. Rev.*, 2005, **249**, 2691–2729.
6 C. Coulon, V. Pianet, M. Urdampilleta and R. Clérac, in *Molecular Nanomagnets and Related Phenomena*, ed. S. Gao, Springer Berlin Heidelberg, Berlin, Heidelberg, 2014, vol. 164, pp. 143–184.
7 C. A. P. Goodwin, F. Ortu, D. Reta, N. F. Chilton and D. P. Mills, *Nature*, 2017, **548**, 439–442.
8 J. M. Frost, K. L. M. Harriman and M. Murugesu, *Chem. Sci.*, 2016, **7**, 2470–2491.
9 F.-S. Guo, B. M. Day, Y.-C. Chen, M.-L. Tong, A. Mansikkamäki and R. A. Layfield, *Science*, 2018, **362**, 1400–1403.
10 T. Tezgerevska, K. G. Alley and C. Boskovic, *Coord. Chem. Rev.*, 2014, **268**, 23–40.

11 Y.-S. Meng, O. Sato and T. Liu, *Angew. Chem. Int. Ed.*, 2018, **57**, 12216–12226.
12 S. Rat, M. Piedrahita-Bello, L. Salmon, G. Molnár, P. Demont and A. Bousseksou, *Adv. Mater.*, 2018, **30**, 1705275.
13 M. Urdampilleta, C. Ayela, P.-H. Ducrot, D. Rosario-Amorin, A. Mondal, M. Rouzières, P. Dechambenoit, C. Mathonière, F. Mathieu, I. Dufour and R. Clérac, *Sci. Rep.,* 2018, **8**, 8016.
14 S. De, L.-M. Chamoreau, H. El Said, Y. Li, A. Flambard, M.-L. Boillot, S. Tewary, G. Rajaraman and R. Lescouëzec, *Front. in Chem.*, 2018, **6**, 326.
15 S. De, S. Tewary, D. Garnier, Y. Li, G. Gontard, L. Lisnard, A. Flambard, F. Breher, M.-L. Boillot, G. Rajaraman and R. Lescouëzec, *Eur. J. Inorg. Chem.*, 2018, 414–428.
16 A. Mondal, Y. Li, P. Herson, M. Seuleiman, M.-L. Boillot, E. Rivière, M. Julve, L. Rechignat, A. Bousseksou and R. Lescouëzec, *Chem. Commun*, 2012, **48**, 5653.
17 A. Mondal, Y. Li, L.-M. Chamoreau, M. Seuleiman, L. Rechignat, A. Bousseksou, M.-L. Boillot and R. Lescouëzec, *Chem. Commun.*, 2014, **50**, 2893–2895.
18 D. Garnier, A. Mondal, Y. Li, P. Herson, L.-M. Chamoreau, L. Toupet, M. Buron Le Cointe, E. M. B. Moos, F. Breher and R. Lescouëzec, *C. R. Chim.*, 2019, **22**, 516–524.
19 S. Kamilya, S. Ghosh, Y. Li, P. Dechambenoit, M. Rouzières, R. Lescouëzec, S. Mehta and A. Mondal, *Inorg. Chem.*, 2020, **59**, 11879–11888.
20 A. Mondal, L.-M. Chamoreau, Y. Li, Y. Journaux, M. Seuleiman and R. Lescouëzec, *Chem. Eur. J.*, 2013, **19**, 7682–7685.
21 A. Mondal, Y. Li, M. Seuleiman, M. Julve, L. Toupet, M. Buron-Le Cointe and R. Lescouëzec, *J. Am. Chem. Soc.* 2013, **135**, 1653–1656.
22 Y. Li, A. Benchohra, B. Xu, B. Baptiste, K. Béneut, P. Parisiades, L. Delbes, A. Soyer, K. Boukheddaden and R. Lescouëzec, *Angew. Chem. Int. Ed.*, 2020, **59**, 17272–17276.
23 Y. Wu, D. Tian, J. Ferrando-Soria, J. Cano, L. Yin, Z. Ouyang, Z. Wang, S. Luo, X. Liu and E. Pardo, *Inorg. Chem. Front.*, 2019, **6**, 848–856.
24 A. Switlicka, B. Machura, R. Kruszynski, N. Moliner, J. M. Carbonell, J. Cano, F. Lloret and M. Julve, *Inorg. Chem. Front.*, 2020, **7**,4535–4552.
25 A. Sarkar, S. Dey and G. Rajaraman, *Chem. Eur. J.*, 2020, **26**, 14058.
26 P. C. Bunting, M. Atanasov, E. Damgaard-Møller, M. Perfetti, I. Crassee, M. Orlita, J. Overgaard, J. van Slageren, F. Neese and J. R. Long, *Science*, 2018, **362**, 7319.
27 J. Vallejo, I. Castro, R. Ruiz-García, J. Cano, M. Julve, F. Lloret, G. De Munno, W. Wernsdorfer and E. Pardo, *J. Am. Chem. Soc.*, 2012, **134**, 15704–15707.
28 S. Tripathi, A. Dey, M. Shanmugam, R. S. Narayanan and V. Chandrasekhar, in *Organometallic Magnets*, eds. V. Chandrasekhar and F. Pointillart, Springer International Publishing, Cham, 2019, pp. 35–75.
29 M.-G. Alexandru, D. Visinescu, S. Shova, A. Bentama, F. Lloret, J. Cano and M. Julve, *Magnetochemistry*, 2020, **6**, 66.
30 P. Alemany, D. Casanova, S. Alvarez, C. Dryzun and D. Avnir, in *Reviews in Computational Chemistry*, eds. A. L. Parrill and K. B. Lipkowitz, John Wiley & Sons, Inc., Hoboken, NJ, USA, 2017, pp. 289–352.
31 L. Banci, A. Bencini, C. Benelli, D. Gatteschi and C. Zanchini, Spectral-Structural Correlation of High-Spin Cobalt(II) Complexes, *Struct. Bonding*, 1982, **52**, 27-86.
32 S. Stoll and A. Schweiger, *J. Magn. Reson.*, 2006, **178**, 42–55.
33 A. Świtlicka, J. Palion-Gazda, B. Machura, J. Cano, F. Lloret and M. Julve, *Dalton Trans.*, 2019, **48**, 1404–1417.
34 A. Paul, M. Viciano-Chumillas, H. Puschmann, J. Cano and S. C. Manna, *Dalton Trans.*, 2020, **49**, 9516–9528.
35 N. F. Chilton, R. P. Anderson, L. D. Turner, A. Soncini and K. S. Murray, *J. Comput. Chem.*, 2013, **34**, 1164–1175.
36 N. F. Chilton, *PHI User Manual* v3.
37 J. - R. Jiménez, M. Tricoire, D. Garnier, L. - M. Chamoreau, J. von Bardeleben, Y. Journaux, Y. Li, and R. Lescouëzec, *Dalton Trans.*, 2017, **46**, ~~44,~~ 15549–15557.
38 A. Zabala-Lekuona, J. M. Seco and E. Colacio, *Coord. Chem. Rev.*, 2021, **441**, 213984.
39 N. Braussaud, T. Rüther, K. J. Cavell, B. W. Skelton and A. H. White, *Synthesis*, 2001, **2001**, 0626–0632.
40 L. J. Farrugia, *J. Appl. Crystallogr.*, 1999, **32**, 837–838.
41 G. M. Sheldrick, *Acta Crystallogr. C Struct. Chem.*, 2015, **71**, 3–8.
42 G. de la Flor, D. Orobengoa, E. Tasci, J. M. Perez-Mato and M. I. Aroyo, *J. Appl. Crystallogr.*, 2016, **49**, 653–664.
43 *CrysAlisPro Software system*, Rigaku Corporation, Oxford, UK, 2015.
44 O. V. Dolomanov, L. J. Bourhis, R. J. Gildea, J. A. K. Howard and H. Puschmann, *J Appl Crystallogr*, 2009, **42**, 339–341.
45 *Diamond - Crystal and Molecular Structure Visualization*, Crystal Impact, H. Putz, Brandenburg, K. Bonn, Germany,
46 F. Neese, *Wires Comput. Mol. Sci.* 2012, **2**, 73–78.
47 F. Weigend and R. Ahlrichs, "Balanced basis sets of split valence, triple zeta valence and quadruple zeta valence quality for H to Rn: Design and assessment of accuracy," *Phys. Chem. Chem. Phys.*, 2005, **7,** 3297-305.
48 A. Schafer, C. Huber and R. Ahlrichs, *J. Chem. Phys.* 1994, **100**, 5829–5835.
49 F. Weigend, "Accurate Coulomb-fitting basis sets for H to Rn," *Phys. Chem. Chem. Phys.*, 2006, **8**, 1057-1065.
50 K. Eichkorn, O. Treutler, H. Ohm, M. Haser and R. Ahlrichs, *Chem. Phys. Lett*. 1995, **242**, 652–660.
51 K. Eichkorn, F. Weigend, O. Treutler, H. Ohm and R. Ahlrichs, *Theor. Chem. Acc*. 1997, **97**, 119–124.
52 S. Kossmann and F. Neese, *J. Chem. Theory Comput*. 2010, **6**, 2325–2338.
53 S. Kossmann and F. Neese, *Chem. Phys. Lett*. 2009, **481**, 240–243.